Sintering of ultrafine undoped SnO_2 powder

E.R. Leite [a,*], J.A. Cerri [a], E. Longo [a], J.A. Varela [b], C.A. Paskocima [b]

[a]*LIEC-DQ-UFSCar, PO Box 676, Sao Carlos, SP, CEP 13565-905, Brazil*
[b]*IQ-UNESP, Araraquara, SP, Brazil*

Abstract

The sintering process of nanometric undoped SnO_2 powder was studied. No macroscopic shrinkage was observed during the sintening process. Grain growth kinetics investigation showed that surface diffusion is the dominant mechanism in the temperature range 500–1300°C. For temperatures higher than 1300°C, high weight loss was measured, suggesting evaporation–condensation as the dominant mass-transport mechanism. Thermogravimetric analysis (TG) and mass spectroscopy studies showed that the surface contamination of the SnO_2 particles by chemical species like H_2O, OH^- and CO_2, has a strong influence on the role of mass transport controlled by surface diffusion. © 2001 Elsevier Science Ltd. All rights reserved.

Keywords: Grain growth; Sintering; SnO_2; Surface diffusion

1. Introduction

Ultrafine powder, formed by nanometric particles (particle size less than 100 nm), can have significant enhanced sintering rates and hence can allow the fabrication of fine grain size full density materials. Considering the Herring model,[1] for similar particle clusters, the mass transport rate is proportional to $1/G^n$, where G is the particle or grain size and (n) is an exponent related to the mass transport mechanism. In this model the values assumed by (n) are two for vapor transport (evaporation/condensation), three for lattice diffusion and four for grain boundary diffusion and surface diffusion. The Herring scale law model predicts that the mass transport rate increases with the decrease in particle size, for both densifying (lattice and grain boundary diffusion) and nondensifying (surface diffusion and evaporation/condensation) mechanisms. Thus, the use of ultrafine powder is not a guarantee to obtain full density material.

Tin oxide (SnO_2) is a typical case where the use of ultrafine powder does not yield a full density material.[2–5] To explain the predominance of the non-densifying mechanism during the sintering process of SnO_2 powder, several models have been proposed.

Santilli et al.[2] proposed that the sintering of SnO_2 xerogel, prepared from a $SnCl_4$ water solution, is based on a non-densifying mechanism that leads to the grain growth process by cluster coalescence. An activation energy of 22 kJ/mol and $n = 6.3$ were reported in this work. Brito et al.,[5] using a SnO_2 powder prepared by a process similar to that used by Santilli et al.,[2] reported a preferential crystallite growth process of the SnO_2 particle in the $<101>$ direction, with an activation energy of 150 kJ/mol and $n = 4$ in this direction. No macroscopic shrinkage was reported.

An analysis of the results reported by Brito,[4,5] and Santilli and co-workers,[2] suggests that the powder morphology, chemical species bonded to the SnO_2 surface and the microstructure of the green pellets have a strong influence on the SnO_2 sintering process. This was also shown by Ahn et al.[6] Powder pressed at 500 MPa with a green density of 55% reached 79% of the theoretical density after sintering at up to 1020°C for 30 min, while powder pressed at 4.5 GPa with a green density of 79% reached 90% of the theoretical density after sintering in the same conditions.

Varela et al.[7] and Kimura et al.[8] proposed a mechanism based on an evaporation/condensation process to explain the grain growth process during the sintering of SnO_2 powder, in a temperature range of 1000–1400°C. In both works no macroscopic shrinkage was observed. Quantum mechanics calculation of SnO_2 clusters, using

* Corresponding author.
E-mail address: derl@power.ufscar.br (E.R. Leite).

semi-empirical and ab-initio methods,[9,10] showed that the bond between Sn–O has a strong covalent behavior. As a consequence the self-diffusion coefficient must be active only at high temperatures, similar to covalent compounds like SiC and Si_3N_4.[11] Analysis of the SnO_2 evaporation process is therefore of fundamental importance. To understand the sintering mechanism, Hoenig and Searcy[12] studied the evaporation process of SnO_2 and reported that at high temperatures this oxide showed a peritectic decomposition according to the reaction:

$$SnO_2 \text{ (s)} \rightarrow SnO \text{ (g)} + 1/2O_2 \text{ (g)} \qquad (1)$$
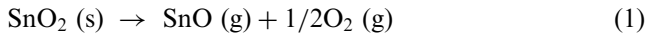
In the temperature range 1200–1700 K, the oxygen partial pressure is given by:

$$\log PO_2 \text{ (atm)} = -2.061 \times 10^{-4}/T + 8.656 \qquad (2)$$

where PO_2 is the oxygen partial pressure and T the temperature. Considering Eq. (2), in Fig. 1 a substantial increase of (PO_2) is observed for temperatures higher than 1200°C, which suggests a high evaporation rate for these temperatures.

The purpose of the present work is to study the sintering process of ultrafine SnO_2 powder, in the temperature range 400–1500°C. This study may contribute to a better understanding of the sintering process of SnO_2 powder and explain why no macroscopic shrinkage is observed during the sintering of tin oxide.

2. Experimental procedure

2.1. Synthesis

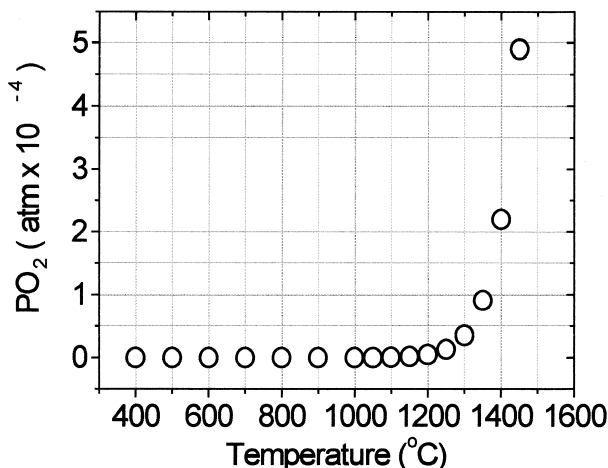Three SnO_2 powders with different particle sizes and post-synthesis thermal treatment were used in this study. Table 1 shows some physical characteristics of the powders used. The powder named S-1 was supplied by Merck (E. Merck, Germany, purity > 99.9%) and was used as received.

The powders S-2 and S-3 were synthesized by the polymeric precursor method using tin citrate aqueous solution, prepared from $SnCl_2.2H_2O$ (Mallinckrodt Baker, USA, purity > 99.9%) and citric acid (E. Merck, Germany, purity > 99.9%). Ethylene glycol was added to the citrate solution, at a mass ratio of 40:60 in relation to the citric acid, to promote a polymerization reaction. After polymerization at 120°C for several hours, the solid resin was treated at 400°C for 2 h. The resulting polymer was ground in a ball mill and calcinated at 500°C for 4 h in air. After this step, the powders were divided into two lots and different heat treatments were performed on each one (post-synthesis treatment). The powder named S-2 was heat-treated at 400°C for 12 h in O_2 flow and the powder named S-3 was heat treated at 400°C, for 12 h in air. Both powders showed a single SnO_2 tetragonal phase with similar surface area after the heat treatment (see Table 1).

2.2. Sintering study

To study the sintering process, the powders were isostatically pressed, attaining a green density of 54% of the theoretical density. The samples were then sintered both in a dilatometer with a heating rate of 10°C/min up to 1550°C (model 402E Netzsch, Germany) and in a tube furnace for an isothermal study. Both experiments were performed in air.

The grain growth kinetics of the sintered pellets was accompanied by measurement of the surface area, using the BET method. The mean grain size was estimated from surface area using the relation:

$$G_{BET} = 6/\rho_T \times S_{BET} \qquad (3)$$

where G_{BET} is the mean grain size, ρ_T the theoretical density, and S_{BET} the surface area.

The crystallite size of the sintered pellets were determined using the diffraction peak of the (110) and (101) SnO_2 planes and the Scherrer equation:

$$G_{DRX} = \lambda K/\beta \cos\theta \qquad (4)$$

Fig. 1. Plot of PO_2 as a function of temperature considering Eq. (2).[12]

Table 1
Characteristics of the powders used in this work

Sample	Surface area (m^2/g)	Average diameter particles (nm)	Average size crystallite (nm)
S-1	10.1	86	55
S-2	34.2	25	12
S-3	36.6	24	12

where λ is the wavelength ($CuK_{\alpha 1}$), θ the diffraction angle, K a constant, and β the corrected half-width of the diffraction peak. In this study, the diffraction peak profile was fitted using a pseudovoigth function to calculate the full width at half maximum (FWHM). Only $CuK_{\alpha 1}$ radiation was considered; $CuK_{\alpha 2}$ radiation was subtracted via computer program software (FIT Program, Diffract AT, Siemens, Germany). The β value was determined considering the following equation:

$$\beta = (B_{0bs}^2 - b^2)^{1/2} \qquad (5)$$

where B_{0bs} is the FWHM that is related to the sample and b is the FWHM of the external standard [quartz (SiO_2)].

Mass spectroscopy coupled to the thermogravimetric analysis system was used to study the chemical desorption during the heat treatment of the pellet isostatically pressed. In this study a heating rate of 10°C/min and high purity He flow were used. Before measurement, samples were degassed at 120°C with steps of vacuum and He flows.

3. Results and discussion

3.1. Weight loss and surface area variation as a function of temperature

The dilatometry results, up to 1550°C, showed no macroscopic shrinkage for all the studied samples. This result is in agreement with previous works[2–5,7,8] that reported no macroscopic shrinkage for pure SnO_2.

Fig. 2 shows the thermogravimetric analysis (TG) of the S-1, S-2 and S-3 samples. In this figure, the existence of two stages of weight loss and one stage of weight gain can be observed, for the three different samples. The first weight loss step, for temperatures up to 600°C, is likely related to the desorption of chemical species bonded
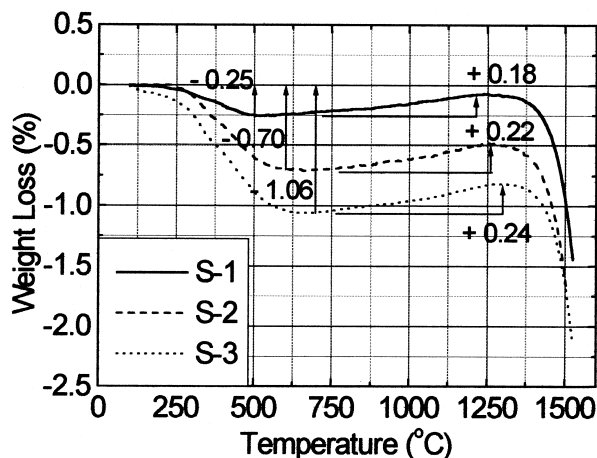
at the SnO_2 surface. In this step the sample S-3 showed the highest weight loss and S-1 the lowest.

The second weight loss step, for temperature above 1300°C, is related to the decomposition process following Eq. (1). Fig. 3 shows that the weight loss rate is similar for all the samples. This result is in agreement with Hoenig and Searcy,[12] who showed a higher decomposition rate of SnO_2 for temperatures above 1300°C. In the weight gain step, between 600 and 1300°C, the sample S-3 showed the higher weight gain (0.26%), following by the sample S-2 (weight gain of 0.20%) and S-1 (gain of 0.15%). This weight gain might be related to annihilation of surface defects by oxygen.

Fig. 4 showed the desorption gas analysis, by mass spectroscopy, of the S-3 sample performed during the TG run. High signal intensities for H_2O, OH^- and CO_2 are observed at temperatures up to 600°C. This result suggests that the weight loss observed in the TG analysis (Fig. 2),
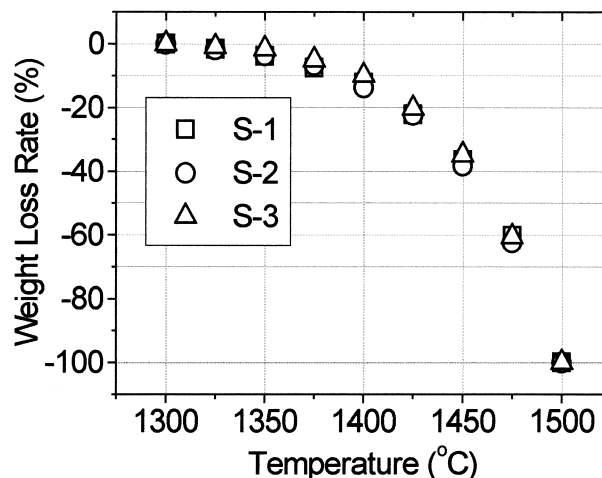

Fig. 3. Weight loss rate for the three samples above 1300°C, indicating the same mass transport mechanism.

Fig. 2. Thermogravimetric analysis (TG) of S-1, S-2 and S-3 samples. Heating rate of 10°C/min, $T_{max} = 1550$°C and He_2 flux of 30 cc/mm.
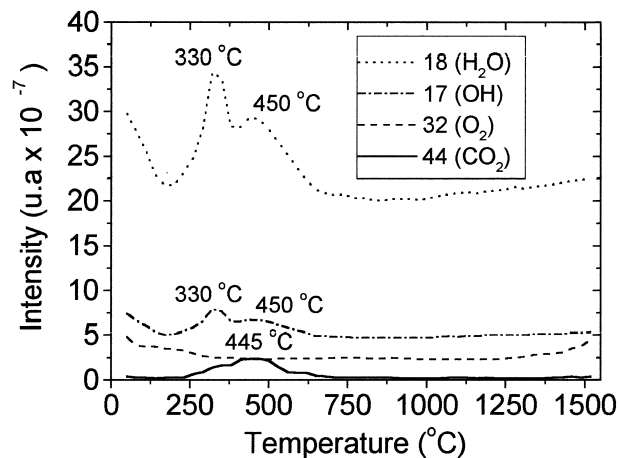

Fig. 4. Mass spectroscopy through gas analysis in S-3 sample, performed during TG run.

is due to the desorption of these chemical species bonded in the SnO_2 surface.

For temperatures higher than 1300°C, an increase in the O_2 signal can be observed in Fig. 4. This result supports the decomposition process to SnO for temperatures above 1300°C. Similar mass spectroscopy results were observed for the S-2 and S-1 samples.

Fig. 5 showed the variation of surface area of the three samples with the increase of temperature. A strong decrease in surface area in the temperature range 400–700°C is observed for the samples S-2 and S-3. A smooth decrease in the surface area with temperature is also observed for the sample S-1 in Fig. 5.

The results showed in the Figs. 2, 4 and 5 suggest that the intensive surface area loss, observed in the samples S-2 and S-3 between 400 and 700°C, is associated with the chemical species desorption, observed in similar temperature range. The desorption of H_2O, OH^- and CO_2, chemically bonded to the surface, likely promotes the formation of oxygen vacancies[13,14] and exposes the intrinsic vacancies. This can lead to an increase in the mass flux, resulting in a decrease of the surface area by neck formation and growth between grains.

As observed in the previous results, higher surface area samples (S-2 and S-3) showed higher weight loss and surface area reduction, in the temperature range 100–700°C, compared with the lower surface area sample (S-1). These results suggest that SnO_2 powder with high surface area will adsorb a large amount of chemical species like H_2O, OH^- and CO_2. During the sintering process, these species will be removed from the SnO_2 surface, increasing the surface defect concentration.

Thus an increase in the mass flux in the surface must occur, promoting a reduction in the surface area. The sample S-2, that was heat treated in O_2 flow, showed less weight and surface area loss compared with sample S-3. The heat treatment in O_2 may have contributed to decrease the concentration of intrinsic defects in the

SnO_2 surface. As a consequence a smaller amount of chemical species will be adsorbed in the surface sample.

At higher temperatures ($T > 1300°C$), all samples showed high weight loss, a strong indication that for temperatures above 1300°C the mass-transport is controlled by evaporation–condensation process.

3.2. Kinetics study

As the samples S-2 and S-3 showed higher surface area variation compared with the sample S-1, a more detailed kinetic study was carried out with these samples.

Considering that the grain size or crystalline size growth follows the empirical equation

$$G^n - G_0^n = kt \tag{6}$$

where G is the grain size or crystallite size, G_0 is the initial grain or crystallite size, k a temperature-dependent constant, t the time and n the growth kinetics exponent. For a thermally activated process, Eq. (6) can be written in the following way:

$$G^n - G_0^n = k_0 \exp(-Q/RT)t \tag{7}$$

where k_0 is a constant, R the gas constant, T the absolute temperature, and Q the activation energy for the mass-transport process. By plotting ($\ln G$) vs $1/T$ for a given time t, the slope will be equal to $-Q/(nR)$. The n value can be obtained by plotting ($\ln G$) vs $\ln t$ for a given temperature. The assumption that $G^n >> G_0^n$ will be considered.

The plot of Fig. 6 shows ($\ln G_{BET}$) as a function of $1/T$ for S-2 and S-3 samples sintered over 2 h, where G_{BET} is the mean grain size that is estimated from Eq. (3). A linear behavior was found for both samples. The plot of ($\ln G_{BET}$) vs $\ln t$ for both samples that have been sintered at 700°C is shown in Fig. 7. The values of n, that
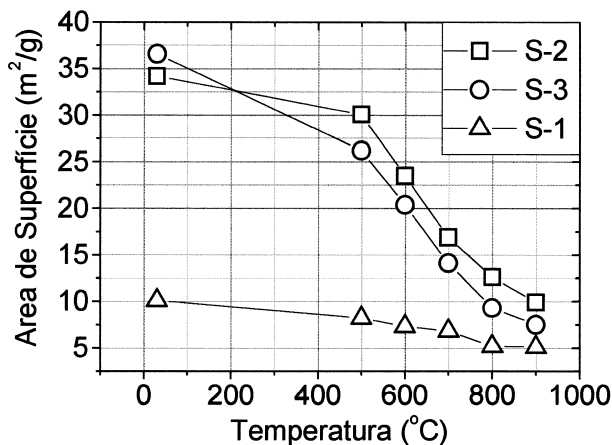

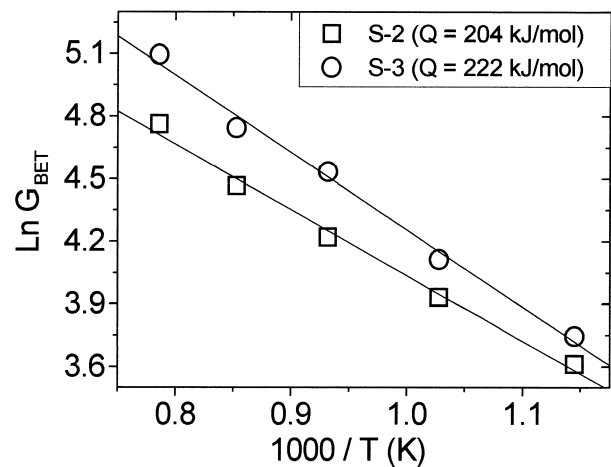Fig. 5. Surface area variation as function of temperature in sintered samples for 2 h.

Fig. 6. Grain growth plot as a function of $1/T$ of samples sintered during 2 h.

were calculated from the slope of the straight line, were 7.8 for the S-2 sample and 7.2 for the S-3 sample. From the values of n and the plots of Fig. 6, the activation energy (Q) for the grain growth estimated by Braunauer, Emmett and Teller (BET) were determined. Q values of 204 kJ/mol for S-2 sample and 222 kJ/mol for S-3 sample were measured. The values of Q and n for both samples can be considered the same within an error smaller than 10%.

A similar procedure was used to analyze the crystallite growth kinetics. The results are showed in Figs. 8 and 9. From these figures, for the sample S-3, the values of $n = 9.6$ and $Q = 349$ kJ/mol in the <110> direction and $n = 10.4$ and $Q = 354$ kJ/mol in the <101> direction were observed. For the sample S-2, values of $n = 12.0$ and $Q = 310$ kJ/mol in the <110> direction and $n = 12.6$ and $Q = 328$ kJ/mol in the <101> were deter-

mined. These results showed that a non-preferential growth was observed for the samples, since the n values in both directions are similar (difference lower than 10%). Similar results were observed by Gouvea et al.[3] in the sintering study of pure SnO_2 synthesized by the same method. The high values determined for n confirm the assumption that $G^n >> G^n_0$.

It can be considered that the grain or crystallite growth rate is proportional to $1/n$ ($dG/dt \propto 1/n$). Taking also into account the kinetics parameters obtained for the grain growth (G_{BET}) and crystallite growth (G_{DRX}) study, is possible to observe that the grain growth rate (dG_{BET}/dt) is higher than the crystallite growth rate (dG_{DRX}/dt). This result is supported by the lower Q value for grain growth (204–222 kJ/mol) compared to the Q value for crystallite growth (310–354 kJ/mol). These results suggest that the mass-transport rate at the surface is higher than in the bulk of the particle. Thus in this temperature range, the mass-transport mechanism must be dominated by surface diffusion.

The variation of grain size (G_{BET}) and crystallite size (G_{DPX}), in the <110> direction as a function of the temperature, for the samples S-2 and S-3 sintered for 2 h is shown in Fig. 10. For temperatures above 600°C, grain sizes are always larger than the crystallite sizes. However, for this temperature range the crystallite size and the grain size are in the same order of magnitude (the ratio $G_{BET}/G_{DRX} < 2$). This suggests that during the sintering process no geometrical changes occur, just an increase in the grain size (change in the scale).

Considering the scale law model, the n value related to surface diffusion is equal to four. In this work values of $n = 7.2$ and 7.8 were measured. This difference can be attributed to surface contamination, likely by chemical species bonded to the powder surface, which can modify the mass-transport rate and hence change the grain size rate and the n value.[1]
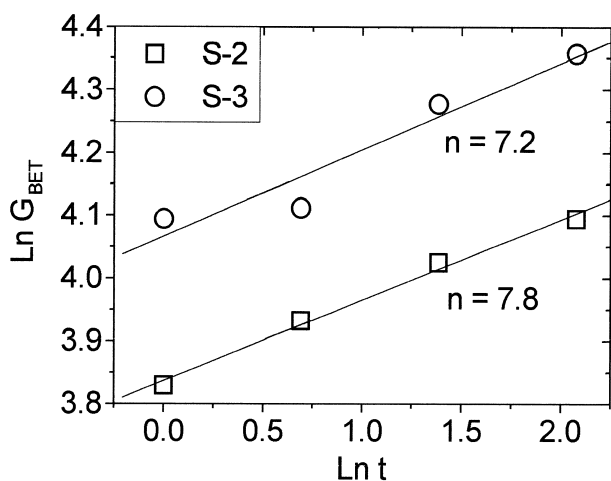

Fig. 7. Plot of exponential coefficient (n) for grain growth of samples sintered at 700°C.
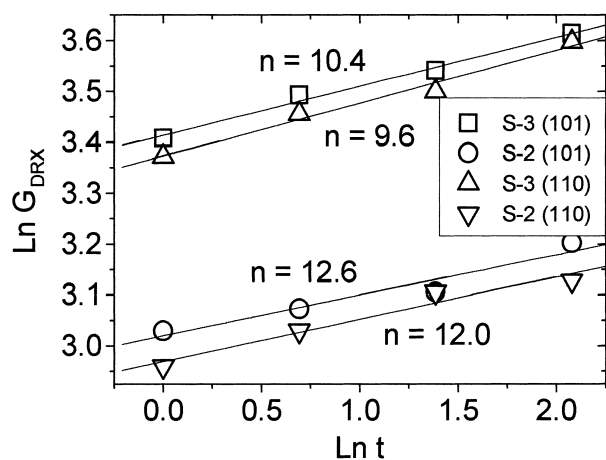

Fig. 8. Plot of exponential coefficient (n) for crystallite growth of samples sintered at 700°C.
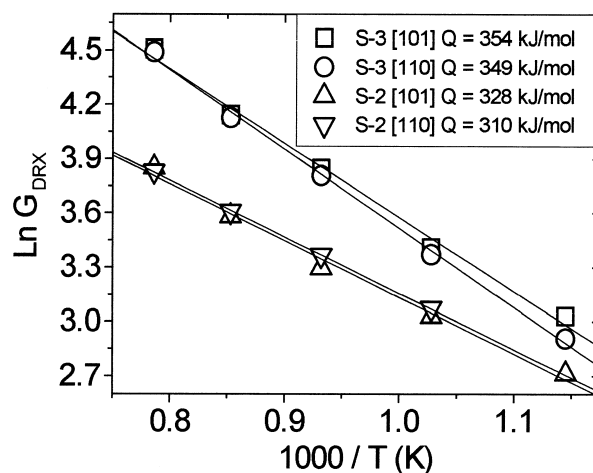

Fig. 9. Crystallite growth plot as a function of $1/T$ of samples sintered for 2 h.
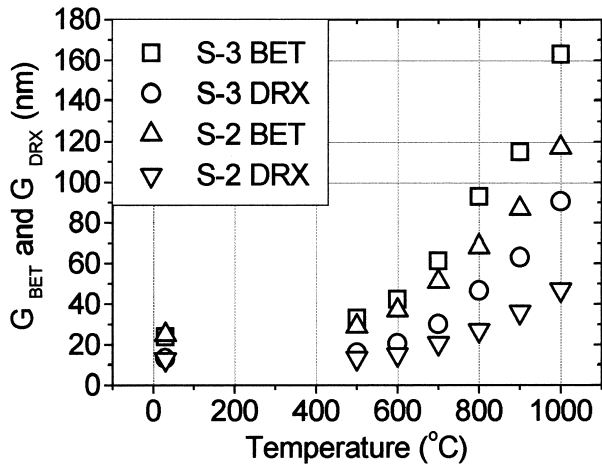
Fig. 10. Relation of grain growth (G_{BET}) and crystallite growth (G_{DRX}) as a function of temperature. The crystallite size was measured in the $<110>$ direction.

3.3. General discussion

The previous results showed that the sintering of pure SnO_2 is controlled by surface diffusion in the temperature range 500–1000°C and by the evaporation–condensation process for temperatures higher than 1300°C. It was also observed that surface contamination has a strong influence in the surface diffusion process. The desorption of chemical species from the surface promotes an increase in the mass-transport rate.

Considering the scale law model, it is possible to assume that the rate of the two dominant mechanisms for SnO_2 sintering vary with the scale of the system according to:

$$(R)_{SD} \; \alpha \; \Lambda_s^{-4} \tag{8}$$

and

$$(R)_{EC} \; \alpha \; \Lambda_s^{-2} \tag{9}$$

where $(R)_{SD}$ is the rate of mass-transport by surface diffusion, $(R)_{EC}$ is the rate of mass-transport by evaporation–condensation and Λ_s is the scale of the system (i.e. related to the grain size).

Fig. 11 shows schematically the variation of the rate of mass-transport with Λ_s for the grain-boundary diffusion mechanism (GB), surface diffusion mechanism (SD), lattice diffusion mechanism (LD) and evaporation–condensation mechanism (E/C). This figure shows that for small Λ_s, the rate of mass-transport by surface diffusion or grain boundary diffusion is enhanced. Conversely, the mass-transport rate by evaporation–condensation dominates for larger Λ_s. Following this analysis and Eqs. (8) and (9), the mass-transport rate during the sintering process of SnO_2 will be dominated by surface diffusion for small grain size and by evaporation–condensation
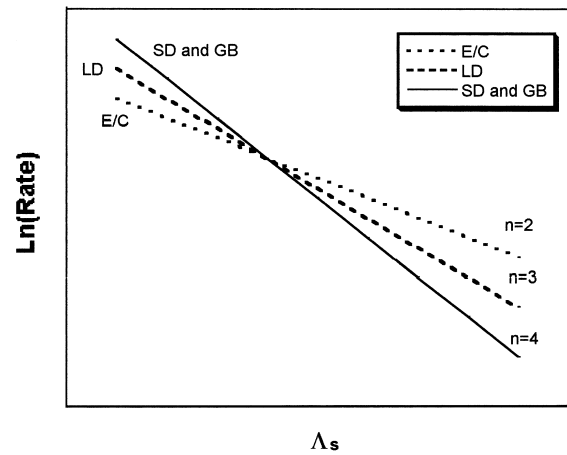

Fig. 11. Schematic representation of mass transport rate as a function of scale factor (Λ_s), considering different mechanisms.

for large grain size, i.e. in high temperature. Thus, the sintering of pure SnO_2 will always be dominated by a non-densifying mechanism.

4. Conclusion

The experimental results that are related to the sintering of nanometric particles of SnO_2 lead to the following conclusion:

1. at low temperature (500° < T < 1000°C), the mass transport mechanism is controlled by surface diffusion;
2. the mass-transport controlled by surface diffusion is very sensitive to the surface contamination. The desorption of chemical species (H_2O, OH^- and CO_2) bonded in the SnO_2 surface modify the mass transport rate;
3. at high temperature (T > 1300°C), the mass transport mechanism is controlled by evaporation–condensation.

References

1. Herring, C., Effect of change of scale on sintering phenomena. *J. Appl. Phys.*, 1950, **21**(4), 301–330.
2. Santilli, C. V., Pulcinelli, S. H. and Craievich, A. F., Porosity evolution in SnO_2 Xerogel during sintering under isothermal condition. *Phys. Rev. B*, 1995, **51**, 8801–8809.
3. Gouvea, D., Varela, J. A., Smith, A. and Bonnet, J. P., Morphological characteristics of SnO_2 based powder containing manganese. *Eur. J. Solid State Inorg. Chem.*, 1996, **t33**, 343–354.

4. Brito, G. E. S., Brios, U., Pulcinelli, S. H. and Santilli, C. V., EXAFS and XRD study of the structural evolution during sintering of SnO₂ Xerogel. *J. Sol–Gel Sci. Technol.*, 1997, **8**, 269–274.

5. Brito, G. E. S., Pulcinelli, S. H. and Santilli, C. V., Anisotropy of crystallite growth during sintering of SnO₂ xerogel. *J. Mater. Sci.*, 1996, **31**, 4087–4092.

6. Ahn, J. P., Park, J. K. and Huh, M. Y., Effect of green density on the subsequent densification and grain growth of ultrafine SnO₂ powder during isochronal sintering. *J. Am. Ceram. Soc.*, 1997, **80**, 2165–2167.

7. Varela, J. A., Whittemore, O. J. and Longo, E., Pore size evolution during sintering of ceramics oxides. *Ceram. Intern.*, 1990, **16**, 177–189.

8. Kimura, T., Inada, S. and Yamaguchi, T., Microstructure development in SnO₂ with and without additives. *J. Mater. Sci.*, 1989, **24**, 220–226.

9. Martins, J. B. L., Modelagem Molecular de Cristais Semiconductores e Estudo de Sua Atividade como Sensores de Gases, PhD Thesis, Chemistry Department, Universidade Federal de Sao Carlos, Brazil, 1995, (in Portuguese).

10. Sensato, F., Internal report (unpublished work), 1996.

11. Greskovich, C. and Rosolowski, J. H., Sintering of covalent solids. *J. Am. Ceram. Soc.*, 1976, **59**, 336–343.

12. Hoenig, C. L. and Searcy, A. W., Knudsen and Langmuir evaporation studies of stannic oxide. *J. Am. Ceram. Soc.*, 1966, **49**, 128–134.

13. Dazhi, W., Shulin, W., Jun, C., Suyvan, Z. and Fangging, L., Microstructure of SnO₂. *Phys. Rev. B*, 1994, **49**, 14282–14285.

14. Fagan, J. G. and Amarakoon, V. R. W., Reliability and reproducibility of ceramic sensors: Part III, humidity sensors. *Am. Ceram. Soc. Bull.*, 1993, **72**, 119–130.